# Plasmon-enhanced optical trapping of metal nanoparticles: force calculations and light-driven rotations of nanoaggregates

O.M. Maragò*[1], R. Saija[2], F. Borghese[2], P. Denti[2], P.H. Jones[3], E. Messina[4], G. Compagnini[4], V. Amendola[5], M. Meneghetti[5], M.A. Iatì[1] and P.G. Gucciardi[1]
[1]Istituto per i Processi Chimico-Fisici (CNR), V.le F. Stagno d'Alcontres 37, I-98158 Messina, Italy
[2]Dip. di Fisica della Materia e Ing. Elettronica, Università di Messina, V.le F. Stagno d'Alcontres 31, I-98166 Messina, Italy
[3]Department of Physics & Astronomy, University College London, Gower Street, WC1E 6BT London, U.K.
[4]Dipartimento di Scienze Chimiche, Università di Catania, Viale A.Doria 6, Catania 95125, Italy
[5]Dipartimento di Scienze Chimiche, Università di Padova, Via Marzolo 1, I-35131 Padova, Italy

## ABSTRACT

We investigate experimentally and theoretically plasmon-enhanced optical trapping of metal nanoparticles. We calculate the optical forces on gold and silver nanospheres through a procedure based on the Maxwell stress tensor in the transition T-matrix formalism. We compare our calculations with experimental results finding excellent agreement. We also demonstrate how light-driven rotations can be generated and detected in non-symmetric nanorods aggregates. Analyzing the motion correlations of the trapped nanostructures, we measure with high accuracy both the optical trapping parameters, and the rotation frequency induced by the radiation pressure.

**Keywords:** Optical trapping, Metal nanoparticles, Plasmon enhancement, Light scattering theory, Light-driven rotations

## 1. INTRODUCTION

Optical tweezers[1] (OT), tools for the trapping and manipulation of micro[2,3] and nanoparticles[4-9], have led to tremendous advances in physics, chemistry, material sciences and biology. OT can measure forces at the femtonewton[4,6] and their integration with Raman spectroscopy (Raman Tweezers) allows for ultra-sensitive chemical-physical analysis of trapped particles[10]. OT have been used to hold and manipulate metal nanoparticles since Svoboda and Block[11]. Manipulating nanoparticles with OT is generally difficult because brownian motion can easily overwhelm the trapping forces. On the other hand the occurrence of plasmon resonances in metal nanoparticles is crucial for enhancing light forces that can stably hold particles as small as 10-20 nm in size[12-18]. Moreover a comprehensive theory of OT for metal particles has only recently been developed[18]. Here we show optical trapping calculations that go well beyond the dipole approximation for gold and silver spherical particles and describe experiments on light-driven rotations on gold nanorods aggregates in an optical trap.

## 2. THEORY OF PLASMON-ENHANCED OPTICAL TRAPPING

### 2.1 Theoretical background

In order to calculate the radiation force on metal nanoparticles we use the full scattering theory in the framework of the transition matrix (T-matrix) approach[19,20]. This approach applies to particles of any shape and refractive index for any choice of the wavelength[7,9,18]. The starting point of our procedure is the formulation by Richards and Wolf[21] of the field configuration in the focal region of a high numerical aperture objective lens in absence of any particle. The resulting field is the field incident on the particle, and the radiation force exerted on it within the region is calculated by resorting to linear momentum conservation for the combined system of field and particle. We adopt a geometry such that the coordinate systems $Oxyz$ is linked to the laboratory and $O'x'y'z'$ to the local frame of reference with origin in the center of mass of the particle[19,20]. Thus the optical force exerted on the particle turn out to be[7,9,18,19,20]:

*marago@me.cnr.it

Optical Trapping and Optical Micromanipulation VII, edited by Kishan Dholakia, Gabriel C. Spalding,
Proc. of SPIE Vol. 7762, 77622Z · © 2010 SPIE · CCC code: 0277-786X/10/$18 · doi: 10.1117/12.863113

$$\mathbf{F}_{\mathrm{Rad}} = r^2 \int_{\Omega} \hat{\mathbf{r}} \cdot \langle \mathsf{T}_{\mathsf{M}} \rangle \, d\Omega \tag{1}$$

where the integration is over the full solid angle, $r$ is the radius of a large sphere surrounding the particle centre of mass, and $\langle \mathsf{T}_{\mathsf{M}} \rangle$ is the time averaged Maxwell stress in the form of Minkowski[22]. No inconvenience comes from this choice because the external medium is isotropic, thus:

$$\langle \mathsf{T}_{\mathsf{M}} \rangle = \frac{1}{8\pi} \mathrm{Re}[n^2 \mathbf{E} \otimes \mathbf{E}^* + \mathbf{B} \otimes \mathbf{B}^* - \frac{1}{2}(n^2 |\mathbf{E}|^2 + |\mathbf{B}|^2)\mathrm{I}] \tag{2}$$

where $\otimes$ denotes dyadic product, $\mathrm{I}$ is the unit dyadic and $n$ is the refractive index of the surrounding medium. When the incident field is a polarized plane wave, the components of the radiation force along the direction of the unit vector $\hat{\mathbf{v}}_{\xi}$ are given by[20]:

$$\mathbf{F}_{\mathrm{Rad}\,\xi} = -\frac{r^2}{16\pi} \mathrm{Re} \int (\hat{\mathbf{r}} \cdot \hat{\mathbf{v}}_{\xi})[n^2(|\mathbf{E}_{\mathrm{S}}|^2 + 2\mathbf{E}_{\mathrm{I}} \cdot \mathbf{E}_{\mathrm{S}}) + (|\mathbf{B}_{\mathrm{S}}|^2 + 2\mathbf{B}_{\mathrm{I}} \cdot \mathbf{B}_{\mathrm{S}})] \, d\Omega \tag{3}$$

where $\mathbf{E}_I$ and $\mathbf{B}_I$ are the incident fields, while $\mathbf{E}_S$ and $\mathbf{B}_S$ are the fields scattered by the particle. Expanding the incident field in a series of vector spherical harmonics with (known) amplitudes $W^{p}_{\mathrm{I}\,lm}$, the scattered field can be expanded on the same basis with amplitudes $A^{p'}_{l'm'}$. The relation between the two amplitudes is given by

$$A^{p'}_{l'm'} = \sum_{plm} S^{p'p}_{l'm'lm} W^{p}_{\mathrm{I}\,lm} \tag{4}$$

where $S^{p'p}_{l'm'lm}$ is the T-matrix of the particle.

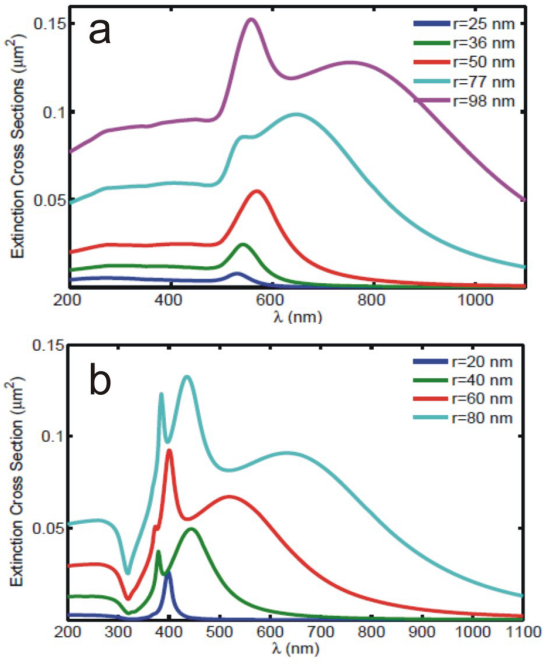


Figure 1. Extinction cross section of Au (a) and Ag (b) spheres. The refractive index is the one tabulated by Johnson and Christy[24].

The elements of the T-matrix are calculated in a given frame of reference through the inversion of the matrix of the linear system obtained by imposing to the fields boundary conditions across each spherical surface[19]. Each element of the T-matrix turns out to be independent both on the direction of propagation and on the polarization of the incident field. Thus they do not change when the incident field is a superposition of plane waves with different direction of propagation, i.e. for the description of a focused laser beam in the angular spectrum representation[26].

### 2.2 Comparison with optical trapping experiments

When comparing calculations of radiation force with experiments, a critical point is the knowledge of the dielectric properties of the particles. In our specific case, we compare our calculations with experiments for gold[12] and silver[15] spheres that were trapped with laser source at $\lambda$=1064 nm. Therefore, we chose, both for gold and silver nanospheres, the dielectric function tabulated by Johnson and Christy[24], whose use leads to a good agreement between calculated and experimental extinction spectra of such nanoparticles. In Fig. 1 we show these calculated extinction cross sections of gold and silver nanospheres of various sizes. The main feature of both metals is the structure of the plasmon resonances whose position and complexity depends on the radius of the particles. We also notice that at 1064nm both gold particles with $r$=77nm and silver particles with $r$=80nm still show a large extinction in comparison with particles of smaller radius.

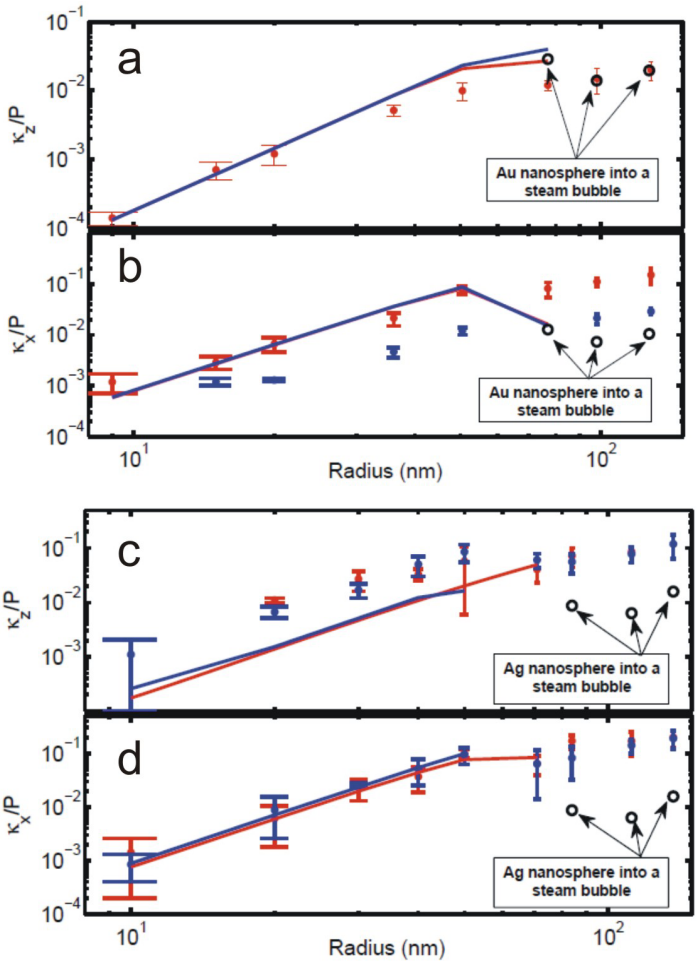


Figure 2. Experimental (from Hansen et al.[12]) and calculated stiffness k$z/P$ (a) and k$x/P$ (b) in pN/(nm·W) for gold spheres, both for water immersion (red line and points) and for oil immersion lens (blue lines and points). The points marked by an arrow refer to particles embedded into a steam bubble. Experimental (from Bosanac et al.[15]) and calculated stiffness k$z/P$ (c) and $\kappa x/P$ (d) in pN/(nm·W) for silver spheres, both for water immersion (red lines and points) and for oil immersion lens (blue lines and points). The points marked by an arrow refer to particles embedded into a steam bubble.

The other parameters (e.g. objective lens type and numerical aperture) that we adopt in our calculations are those of Hansen et al.[12] for gold and of Bosanac et al.[15] for silver. Since trapping particles of different size require different laser power, the experimental stiffnesses of the trap are normalized to the laser power $P$. In Fig. 2 we show our calculated stiffnesses $k_z/P$ and $k_x/P$ as a function of sphere radii together with the experimental data for both gold and silver. We see that our calculations do not account for the trapping of spheres with $r > 77$nm, whereas experiments demonstrated the ability to trap gold spheres with $r$ up to 127nm and silver spheres with $r$ up to 137.5nm, respectively. Nevertheless, in [12] the authors stress that they were unable to get stable trapping of gold spheres with $r = 77$nm, whereas Bosanac et al.[15] notice that their measured stiffnesses for silver spheres with $r = 80$nm are much lower than expected. In fact, this is not surprising, because the experimental measurements include all effects, linear and nonlinear, yielded by the radiation field with scarce or no possibility of discrimination. On the other hand, our calculations are performed for fixed parameters of the model, i.e., fixed radius and refractive index of the particles, and fixed refractive index of the surrounding medium. We note that in the axial direction our calculated spring constants $k_z/P$ are in a very good agreement with the experimental data up to radii at which trapping is predicted by the theory. A fair agreement is also attained for the axial trapping of silver. Our results for the radial axis $k_x/P$ in Fig. 2 show that the calculated curves for non-aberrated and aberrated setup are quite superposed, and agree rather well with the experimental data for the non-aberrated setup. In Fig. 2 a clear size scaling is evident for small radii. The optical trapping stiffnesses lie on mutually parallel lines with slope 3 on a log-log scale, thus showing the existence of a scaling law with the volume of the particle. The fact that our calculated results change their slope for radii larger than 50 nm suggests the transition from a proportionality to the volume to a dependence on some other feature. Indeed, in the range of radii between 70 and 80 nm there occur a change in the trapping regime due to an increase in the scattering processes that weakens the trapping.

The behavior of the radiation force in the region in which the trapping of spheres with $r > 80$nm might occur, strongly suggests that a given model with fixed parameters (i.e. without dynamics) cannot explain the trapping of the larger particles: the theory is linear in the power, indeed. We must thus consider the possibility that the parameters of the model, essentially the refractive index, may change with increasing power. In this respect, it is quite natural to suspect the heating both of the medium and of the particles due to the use of a large laser power. We have use a simplified model for metal particles surrounded by a steam bubble that consequently changes the dielectric constants of the core-shell structure subject to the trapping beam. The calculated trap stiffnesses for such models are reported and marked by arrows in Fig. 2 for gold (a,b) and for silver (c,d). We see at once that our calculated values of $k_z/P$ for gold, rather surprisingly, coincide with the experimental values. In particular the addition of the bubble to the 77 nm spheres produces little change of $k_z/P$. As for $k_x/P$, we see that for 77 nm spheres it lies on the calculated curve, whereas, for the largest spheres, it lies on a line parallel to the experimental data. On the other hand, for silver (Fig. 2c,d) we see that the calculated stiffnesses in the presence of a steam bubble are rather lower than the experimental data. In a sense this confirms the finding of Bosanac et al.[15] that the experimental stiffnesses for these spheres turn out to be lower than expected.

## 3. LIGHT-DRIVEN ROTATIONS IN NANORODS AGGREGATES

### 3.1 Optical rotation of gold nanorods

We consider the trapping, alignment and steady-state optically driven rotation of noble metal nanoparticles, and the quantitative measurement of rotation by analysis of the particle tracking signals. Our samples consist of 10 nm × 45 nm gold nanorods (Nanopartz) dispersed in water with a Cetyl trimethylammonium bromide (CTAB) surfactant. The measured extinction spectrum of the gold nanorods, shown in Fig. 3(a), reveals a plasmon wavelength of 780nm. For our experiments the trap laser wavelength of 830 nm (shown with a red line in Fig 3(a)) is red-detuned relative to the plasmon resonance which leads to local field enhancement and consequently an increased optical force[8,14,16]. A few tens of microliters of the nanoparticle solution is placed in a 75 μl chamber attached to a piezo-stage with 1 nm resolution. The stage is used to steer nanoparticles close to the diffraction-limited laser beam waist where they are trapped. The behavior of nanostructures in an optical trap depends on their physical and optical properties. For one dimensional nanostructures with a transverse dimension $d \ll \lambda$, the orientation in the trap depends on the particle length $L$, which determines the balance of optical torques that control the alignment. For dielectric particles this has been shown to exhibit a critical behavior at $L = 0.36\lambda$ [7]. Experimentally, for a trapping wavelength in the near infrared, nanostructures longer than approximately 300 nm align with the laser propagation direction[4,6,7] whereas shorter ones align transversely to the trap axis and parallel to the dominant polarization direction[7]. In our experiment we observe the trapping of *aggregates* of gold nanorods. Although the dimensions of the aggregates exceeds the critical value for axial alignment,

the individual rods are shor, and the trapping forces and effects of polarization alignment are enhanced by the proximity of the laser wavelength to the rod plasmon resonance[8,14,16] resulting in alignment parallel to the dominant polarization direction and transverse to the trap axis. The trap laser polarization direction can be changed by rotating a half-wave plate in the beam path., hence controlled rotation of an ellipsoidal aggregate of gold nanorods is possible, as in Figure 3(b,c).

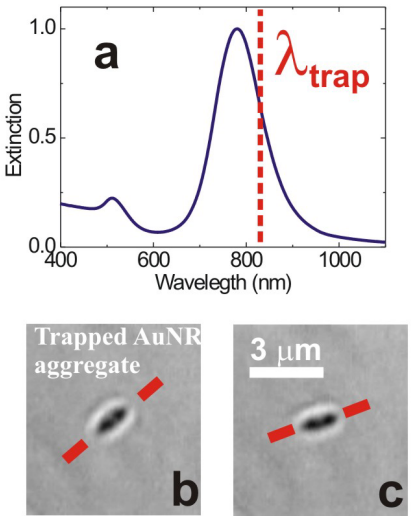


Figure 3. (a) extinction spectrum of gold nanorods, showing the plasmon resonance. The trapping laser wavelength is indicated by the red dashed line. (b,c) Images of an optically trapped aggregate. This aligns with the long axis parallel to the polarization of the trapping beam and is rotated by turning a half wave plate in the beam path.

Continuous rotation in the optical trap is observed for aggregates of gold-nanorods with an asymmetric morphology. We use one with an asymmetric T-shape as sketched in Figure 4(a). When trapped this orients with its plane perpendicular to the trap axis (indicated by $\underline{\boldsymbol{k}}$). We contrast this with the larger polymer cross object used in Galajda et al. [25] which was aligned with its plane containing the trap axis. In the case of asymmetric objects rotation can arise from unbalanced radiation pressure (*windmill effect*)[26]. The gold aggregate also experiences an additional torque due to form birefringence, as it attempts to align the long axis with the laser polarization. This effect is further enhanced by the proximity of the trapping wavelength to the gold nanorod plasmon resonance with the result that the structure is set it into rapid rotation, as seen in the frames of Figure 4(b,c).

### 3.2 Correlation function analysis of rotation

Due to the high rotation frequency of the trapped nanostructures, video microscopy is not suitable for measuring the rotation speed, as only an average image over the exposure time of each frame is recorded. We therefore use a method based on recording an interferometric particle tracking signal and evaluating the correlations between the motions in orthogonal directions[8]. The interference pattern between forward-scattered and unscattered light in the back aperture of the microscope condenser is imaged onto a quadrant photodiode (QPD) from which tracking signals are derived that reveal the particle's motion in the trap[8,27]. The frequency response of this technique is limited by the bandwidth of the electronics that records the tracking signal (approximately 100 kHz in our experiment), therefore enabling detection of much higher rotational frequencies. Furthermore, the same laser beam that drives the nanostructure's rotation is also used for the detection of that motion, thus considerably simplifying the experimental geometry.

An example of the particle tracking signal of the T-shaped nanostructure from one axis is plotted in Figure 4(d) and can be seen to exhibit a strong modulation due to the nanostructure's rotation. We explain the form of the gold nanoaggregate tracking signals by considering an asymmetric planar structure rotating in the optical trap potential about the *z*-axis at a frequency Ω. There are thus two contributions to the interference pattern, symmetric and non-symmetric with respect to a main axis, and rotating in the *xy* plane. The non-symmetric part rotates at a frequency Ω, whereas the symmetric part leads to a signal modulation at a frequency 2Ω. Thus, we can write the resulting QPD tracking signals for motion in the transverse plane as:

$$S_x(t) \propto x(t) + A\cos(\Omega t) + B\cos(2\Omega t) \tag{5}$$

$$S_y(t) \propto y(t) + A\sin(\Omega t) + B\sin(2\Omega t) \tag{6}$$

where $x$, $y$ are the center-of-mass coordinates, and $A$, $B$ constants related to the structure geometry. Recalling the stochastic nature of the center-of-mass $x_i$ coordinates, it is possible to show that the autocorrelations of the tracking signals in Equations (5, 6) are:

$$C_{xx}(\tau) \propto \left[ \left\langle x(t)x(t+\tau) \right\rangle + \frac{A^2}{2}\cos(\Omega t) + \frac{B^2}{2}\cos(2\Omega t) \right] \tag{7}$$

$$C_{yy}(\tau) \propto \left[ \left\langle y(t)y(t+\tau) \right\rangle + \frac{A^2}{2}\cos(\Omega t) + \frac{B^2}{2}\cos(2\Omega t) \right] \tag{8}$$

where the first term in each expression ($\left\langle x(t)x(t+\tau) \right\rangle$ and $\left\langle y(t)y(t+\tau) \right\rangle$) is the autocorrelation of the corresponding centre-of-mass fluctuations. It may be shown that these are exponentially decaying function of lag time, $\tau$, with characteristic time $(\kappa\Gamma)^{-1}$, where $\Gamma$ is the hydrodynamic mobility coefficient[4,6,8] and $\kappa$ the trap spring constant in that direction.

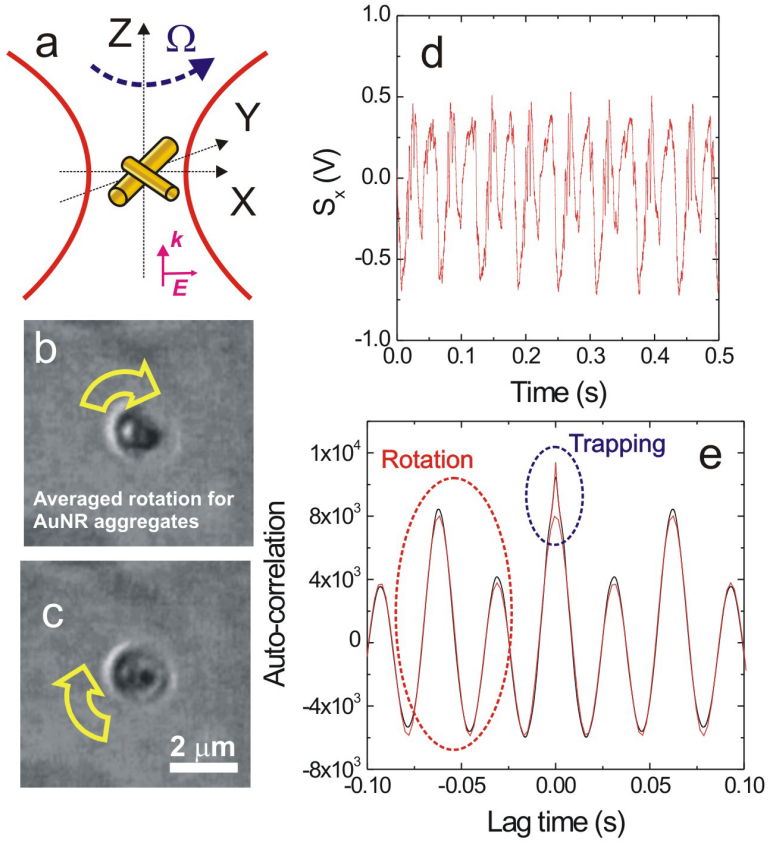


Figure 4. (a) Geometry and trapping orienation of a T-shaped gold nanorods aggregate. (b,c) Video frames showing the nanorods rotation. (d) Tracking signal of the projection of the aggregate onto the $x$ direction, which oscillates as the aggregate rotates. (e) Autocorrelation of the gold nanorod aggregate tracking signals ($Cxx$) showing sinusoidal modulation due to rotation, and, at short times, exponential decay due to trapping.

The subsequent terms in the autocorrelation functions arise from the rotational motion in the trap which produce oscillations at Ω from the non-symmetric part, and 2Ω from the symmetric part. Similarly, the *cross*-correlation of the transverse direction tracking signals isolates the oscillations related to optically induced rotation in quadrature with the autocorrelation because of the stochastic nature of the center-of-mass co-ordinates that are uncorrelated[4,6,8]. An example of the auto-correlation of tracking signals for the gold nanorod aggregate is shown in Figure 4(e) which shows the two-frequency sinusoidal oscillation expected from the analysis above. A fit with functions of the form of Equations (7, 8) yields a rotation frequency $\Omega = 101.6 \pm 0.1$ rad/s and an exponential decay in the region of $\tau = 0$, with a relaxation frequency $\omega = 476 \pm 5$ rad/s.

## 4. CONCLUSIONS

In conclusions we have shown that an electromagnetic theory that goes beyond the dipole approximation is able to give a reliable quantitative interpretation of optical trapping experiments on gold and silver nanospheres. We find excellent agreement for particles with size below 160 nm, while for larger particles we rely on a simplified model that includes bubble formation around the metal spheres. Although our model should be considered as a working hypothesis, it definitely gives an acceptable agreement with the available experimental data.

We have also studied self-assembled gold nano-aggregates whose shape gives rise to continuous rotation in the optical tweezers. Trapping, rotation and motion detection were performed simultaneously with a single laser beam using the methods of back focal plane interferometry for particle tracking, and correlation function analysis of the tracking signals enabled the optical trapping parameters and speed of rotation to be quantified. This method is universal and can be applied to particles of arbitrary shape or microfabricated elements[28]. We expect that these results will enable real-time monitoring and control of optically assembled and light-driven nanomachines by all-optical methods, thus taking a significant step toward enabling the integration of such a system into, for example, lab-on-a-chip devices where trapped nanostructures may act as rotational probes or as light-driven nanopumps.

## REFERENCES


[1] Ashkin, A., Dziedzic, J. M., Bjorkholm, J. E., Chu, S. "Observation of a single-beam gradient force optical trap for dielectric particles." Opt. Lett. 11, 288 (1986).

[2] Ashkin A., "Optical Trapping and Manipulation of Neutral Particles Using Lasers", World Scientific Publishing, Singapore, (2006).

[3] Grier, D.G. "A revolution in optical manipulation" Nature, 424, 810-816 (2003).

[4] Maragò, O.M.; Jones, P.H.; Gucciardi, P.G. "Photonic Force Microscopy: From Femtonewton Force Sensing to Ultra-Sensitive Spectroscopy" in Scanning Probe Microscopy in Nanoscience and Nanotecnology, ed. B. Bushan, Springer-Verlag, (2010).

[5] Nakayama, Y. et al., "Tunable nanowires nonlinear optical probe." Nature, 447, 1098-1102 (2007).

[6] Maragò, O.M.; et al., "Femtonewton Force Sensing with Optical Trapped Nanotubes." Nano Lett., 8, 3211-3216 (2008).

[7] Borghese F.; et al., "Radiation force and torque on optically trapped linear nanostructures", Phys. Rev. Lett., 100, 163903 (2008).

[8] Jones, P.H.; et al., "Rotation detection in light-driven nanorotors", ACS Nano, 3, 3077-3084 (2009).

[9] Neves, A.A.R.; et al., "Rotational dynamics of optically trapped nanofibers", Opt. Express, 18, 822-830 (2010).

[10] Petrov, D.V. "Raman spectroscopy and optically trapped particles." J. Opt. A: Pure Appl. Opt., 9, S139-S156 (2007).

[11] Svoboda, K.; Block, S. M. "Optical trapping of metallic Rayleigh particles". Opt. Lett. 28, 930-932 (1998).

[12] Hansen, P.M.; Bhatia, V. K.; Harrit, N.; Oddershede L. "Expanding the optical trapping range of gold nanoparticles." Nano Lett. 5, 1937-1942 (2005).

[13] Seol, Y; Carpenter, A.E.; Perkins, T.T. "Gold nanoparticles: enhanced optical trapping and sensitivity coupled with significant heating." Opt. Lett. 31, 2429-2431 (2006).

[14] Pelton, M.; et al.; "Optical trapping and alignment of single gold nanorods by using plasmon resonances", Opt. Lett., 31, 2075 (2006).

[15] Bosanac, L.; Aabo, T.; Bendix, P.M.; and Oddershede, L.B. "Efficient optical trapping and visualization of silver nanoparticles", Nano Lett., 8, 1486-1491 (2008).

[16] Selhuber-Unkel, C.; et al. "Quantitative optical trapping of single gold nanorods", Nano Lett., 8, 2998-3003 (2008).
[17] Hajizadeh, F.; Nader, S.; Reihani, S. "Optimized optical trapping of gold nanoparticles." Opt. Exp. 18, 551-559 (2010).
[18] Saija, R.; Denti, P.; Borghese, F.; Maragò, O.M.; Iatì, M.A. "Optical trapping calculations for metal nanoparticles. Comparison with experimental data for Au and Ag spheres." Opt. Exp. 17, 10231-10241 (2009).
[19] Borghese, F., Denti, P., Saija, R. "Scattering from model nonspherical particles", Springer, Berlin, 2nd ed. (2007).
[20] Borghese, F., et al., "Optical trapping of nonspherical particles in the T-matrix formalism", Opt. Express 15, 11984–11998 (2007).
[21] Richards, B., and Wolf, E. "Electromagnetic diffraction in optical systems II. Structure of the image field in an aplanatic system." Proc. R. Soc. London Ser. A, 253, 358 (1959).
[22] Pfeifer, R.N., et al., "Momentum of an electromagnetic wave in dielectric media." Rev. Mod. Phys. 79, 1197-1216 (2007)
[23] Novotny, L., and Hecht, B. "Principles of Nano-Optics", Cambridge University Press, New York, (2006).
[24] Johnson, P. B., Christy, R. W. "Optical constants of the noble metals", Phys. Rev. B 6, 4370–4379 (1972).
[25] Galajda, P., Ormos, P. "Orientation of Flat Particles in Optical Tweezers by Linearly Polarized Light" Opt. Express 11, 446–451 (2003).
[26] La Porta, A., Wang, M. D. "Optical Torque Wrench: Angular Trapping, Rotation, and Torque Detection of Quartz Microparticles", Phys. Rev. Lett. 92, 190801 (2004).
[27] Volpe, G., Petrov, D. "Torque Detection Using Brownian Fluctuations." Phys. Rev. Lett. 97, 210603 (2006).
[28] Galajda, P., Ormos, P. "Complex Micromachines Produced and Driven by Light." Appl. Phys. Lett. 78, 249–251 (2001).